arXiv:1004.4067v1 [physics.acc-ph] 23 Apr 2010

DEUTSCHES ELEKTRONEN-SYNCHROTRON

Ein Forschungszentrum der Helmholtz-Gemeinschaft

DESY 10-053

April 2010

A simple method for controlling the line width of SASE X-ray FELs

Gianluca Geloni,
European XFEL GmbH, Hamburg

Vitali Kocharyan and Evgeni Saldin
Deutsches Elektronen-Synchrotron DESY, Hamburg

ISSN 0418-9833

NOTKESTRASSE 85 - 22607 HAMBURG

A simple method for controlling the line width of SASE X-ray FELs

Gianluca Geloni, [a,1] Vitali Kocharyan [b] and Evgeni Saldin [b]

[a] *European XFEL GmbH, Hamburg, Germany*

[b] *Deutsches Elektronen-Synchrotron (DESY), Hamburg, Germany*

Abstract

This paper describes a novel single-bunch self-seeding scheme for generating highly monochromatic X-rays from a baseline XFEL undulator. A self-seeded XFEL consists of two undulators with an X-ray monochromator located between them. Previous self-seeding schemes made use of a four-crystal fixed-exit monochromator in Bragg geometry. In such monochromator the X-ray pulse acquires a cm-long path delay, which must be compensated. For a single-bunch self-seeding scheme this requires a long electron beam bypass, implying modifications of the baseline undulator configuration. To avoid this problem, a double bunch self-seeding scheme based on a special photoinjector setup was recently proposed. At variance, here we propose a new time-domain method of monochromatization exploiting a single crystal in the transmission direction, thus avoiding the problem of extra-path delay for the X-ray pulse. The method can be realized using a temporal windowing technique, requiring a magnetic delay for the electron bunch only. When the incident X-ray beam satisfies the Bragg diffraction condition, multiple scattering takes place and the transmittance spectrum in the crystal exhibits an absorption resonance with a narrow linewidth. Then, the temporal waveform of the transmitted radiation pulse is characterized by a long monochromatic wake. The radiation power within this wake is much larger than the shot noise power. At the entrance of the second undulator, the monochromatic wake of the radiation pulse is combined with the delayed electron bunch, and amplified up to saturation level. The proposed setup is extremely simple and composed of as few as two simple elements. These are the crystal and the short magnetic chicane, which accomplishes three tasks by itself. It creates an offset for crystal installation, it removes the electron micro-bunching produced in the first undulator, and it acts as a delay line for temporal windowing. Using a single crystal installed within a short magnetic chicane in the baseline undulator, it is possible to decrease the bandwidth of the radiation well beyond the XFEL design down to 10^{-5}. The installation of the magnetic chicane does not perturb the undulator focusing system and does not interfere with the baseline mode of operation. We present feasibility study and exemplifications for the SASE2 line of the European XFEL.

1 Introduction

As a consequence of the start-up from shot noise, the longitudinal coherence of X-ray SASE FELs is rather poor compared to conventional optical lasers. The coherence time is defined by the inverse spectral width. For conventional XFELs [1]-[5] this is typically two orders of magnitude shorter than the electron pulse duration. Hence, the typical XFEL pulse bandwidth is about two orders of magnitude larger than the Fourier transform limited value for the total bunch length. Given this physical properties, it is in principle possible to improve the longitudinal coherence and produce X-rays with a bandwidth of about 10^{-5}.

Self-seeding schemes have been studied to reduce the bandwidth of SASE X-ray FELs [6]-[10]. A self-seeded FEL consists of two undulators with an X-ray monochromator located between them. The first undulator operates in the linear high-gain regime starting from the shot-noise in the electron beam. After the first undulator, the output radiation passes through the X-ray monochromator, which reduces the bandwidth to the desired value, smaller than the FEL bandwidth. While the radiation is sent through the monochromator, the electron beam passes through a bypass, which removes the electron micro-bunching introduced in the first undulator and compensates for the path delay created during the passage in the monochromator. At the entrance of the second undulator, the monochromatic X-ray beam is then combined with an electron beam and amplified up to the saturation level. The radiation power at the entrance of the second undulator is dominant over the shot noise power, so that the bandwidth of the input signal is smaller than the bandwidth of the FEL amplifier. The realization of this self-seeding scheme for the European XFEL requires two undulators, the first 54 m long (9 cells) and the second 72 m long (12 cells), separated by a four-crystal, fixed-exit monochromator in reflection (Bragg) geometry. In the monochromator, the X-ray pulse acquires a centimeter-long path delay, which must be compensated. For a single bunch self-seeding scheme this requires a long electron beam bypass with a length of about 60 m, implying modifications of the baseline undulator configuration, Fig. 1. As an attempt to go around this obstacle, a double-bunch self-seeding scheme was proposed in [11], based on a photoinjector setup using a laser pulse doubler [12].

All X-ray crystal monochromators operate in the frequency domain as bandpass filters. In this paper we propose, instead, a new method of monochromatization based on the use of a single crystal in the transmission direction as a bandstop filter. In this way, the problem with the extra path-delay of

[1] Corresponding Author. E-mail address: gianluca.geloni@xfel.eu

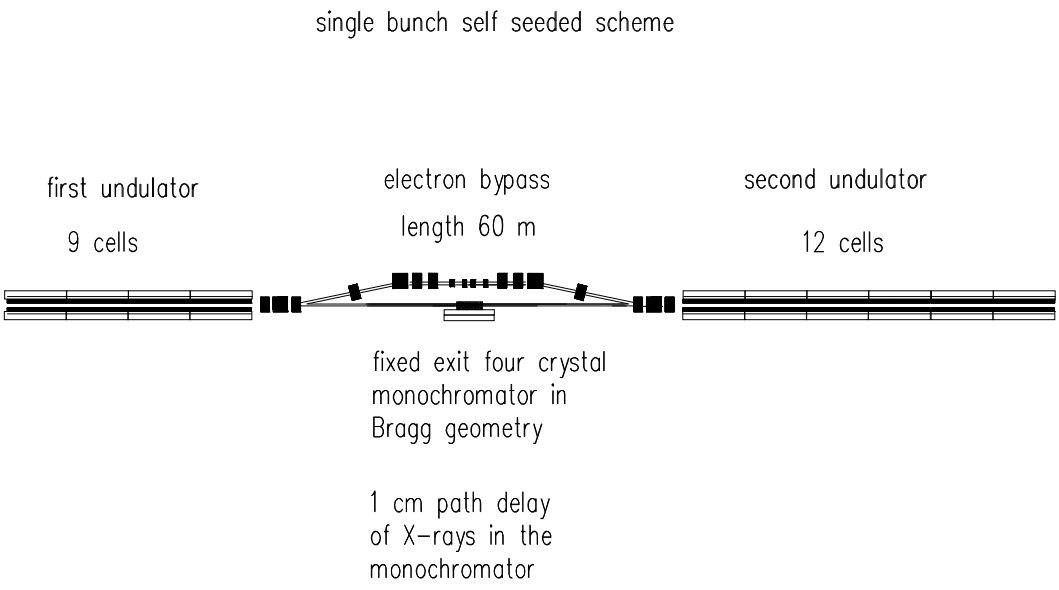

Fig. 1. Design of an undulator system for the narrow bandwidth mode of operation. The scheme is based on the use of a single bunch self-seeding scheme with a fixed-exit four-crystal monochromator in Bragg geometry. The presence of the monochromator introduces a path delay of the X-rays, which has to be compensated with the introduction of a long electron beam bypass.

the X-ray pulse does not exist at all. Our scheme can be realized with the help of a temporal windowing technique. When the incident X-ray beam satisfies the Bragg diffraction condition, multiple scattering takes place in the crystal and the spectrum of the reflectance exhibits a narrow line width. As a consequence, the spectrum of the transmittance exhibits an absorption resonance with a narrow line width, thus behaving as a a bandstop filter. After such bandstop filter, the frequency spectrum of the transmitted X-ray pulse experiences a strong temporal separation. In particular, the temporal waveform of transmitted radiation pulse exhibits a long monochromatic wake. At the entrance of the second undulator, the monochromatic wake of the radiation pulse is combined with the delayed electron bunch, thus exploiting the before-mentioned temporal windowing technique, and it is amplified up to saturation. The wake power is dominant over the shot noise power, so that the bandwidth of the input signal is small, compared to the bandwidth of the FEL amplifier.

The proposed setup is extremely simple, and is composed of two simple elements: a crystal, Fig. 2, and a short magnetic chicane, Fig. 3. The magnetic chicane accomplishes three tasks. It creates an offset for the crystal installation, it removes the electron microbunching produced in the first undulator, and it acts as a delay line for the implementation of the temporal windowing. Thus, using a single crystal installed within a short magnetic chicane in the baseline undulator as a bandstop filter, it is possible to decrease the

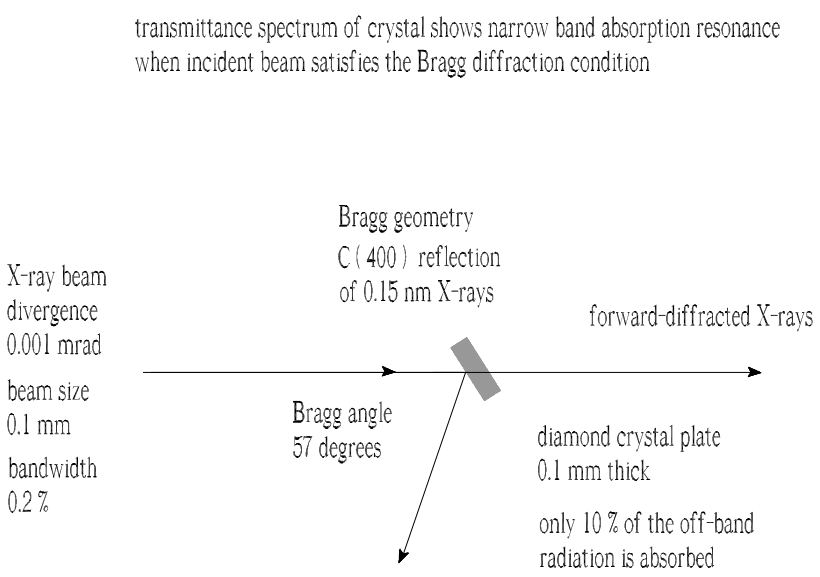

Fig. 2. Forward diffraction in a single crystal in Bragg geometry. Due to multiple scattering, the transmittance spectrum in a crystal shows an absorption resonance with a narrow (10^{-5}) linewidth. Resonant wavelength and incident angle of the X-ray beam satisfy the Bragg diffraction condition. When the incident angle and the spectral contents of the incoming beam satisfies the Bragg diffraction condition, the temporal waveform of the transmitted radiation pulse exhibits a long monochromatic wake. The duration of the wake is inversely proportional to the bandwidth of the absorption resonance.

bandwidth of the radiation well beyond the XFEL design down to 10^{-5}. The installation of the magnetic chicane does not perturb the undulator focusing system and does not interfere with the baseline mode of operation. The scheme can work in combination with a fresh bunch technique [13]-[20] both for short (6 fs) and long (60 fs) pulse mode of operation.

2 Principles of the self-seeding technique based on the use of a wake monochromator

In this section we illustrate our novel method of monochromatization, based on the use single crystal monochromator. As already said, this technique takes advantage of the transmission geometry, where no extra path-delay for the X-ray pulse is present. The method consists of a combination of a single bunch self-seeding scheme, based on the use of a single crystal monochromator, and of a temporal windowing technique.

The principle of the new method of monochromatization is very simple and is illustrated in Fig. 4 and Fig. 5. An incident SASE pulse coming from

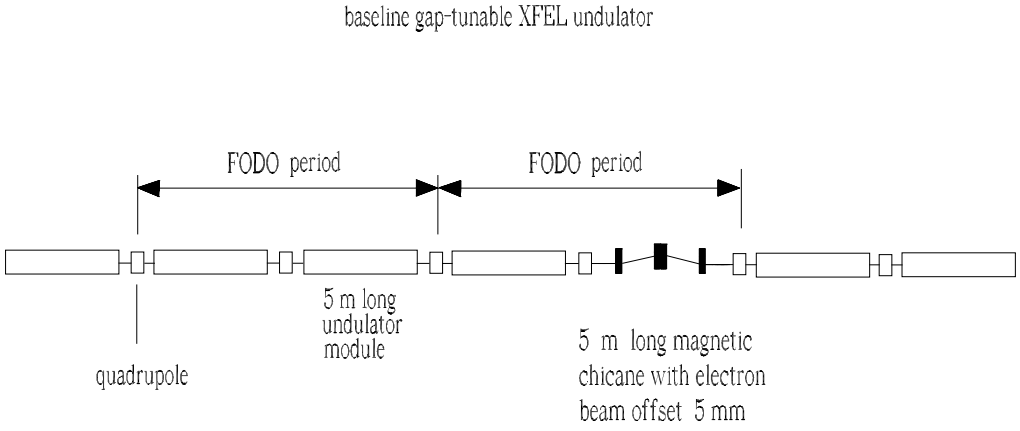

Fig. 3. Installation of the magnetic chicane in the baseline XFEL undulator. The magnetic chicane absolves three tasks. First, it suppresses the electron beam modulation. Second, it allows for the installation of the single-crystal filter. Third, it performs a temporal windowing operation by delaying the bunch.

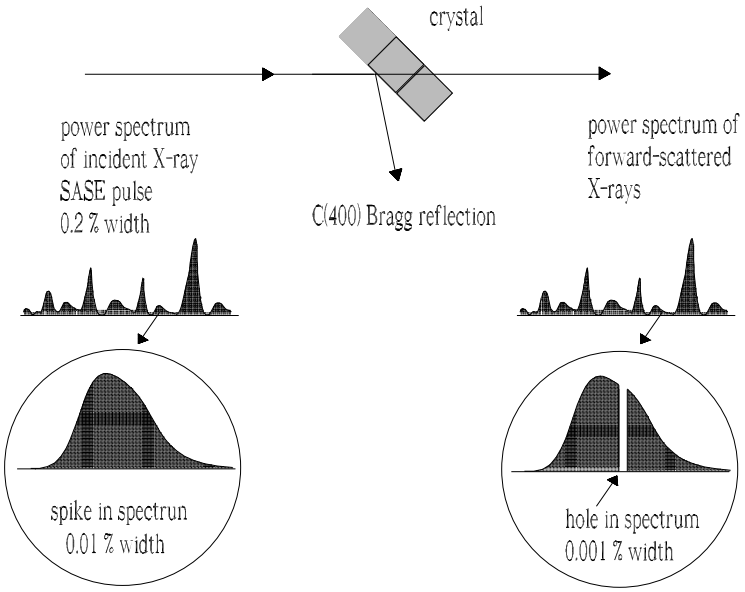

Fig. 4. Single crystal in Bragg geometry as a bandstop filter for the transmitted X-ray SASE radiation pulse.

the first undulator impinges on a crystal set for Bragg diffraction. When X-rays impinge upon a crystal, forward-scattered X-rays are produced. The phase shift acquired by the forward-scattered X-rays on the passing through the crystal depends on the refractive index of the crystal. In general, the refractive index is slightly less than unity and complex. The refractive index,

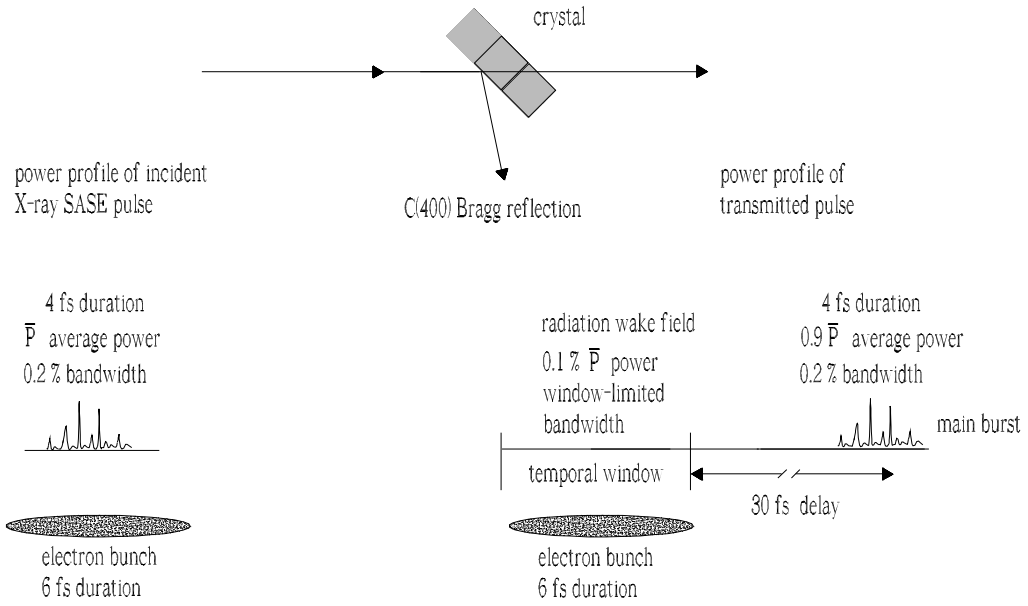

Fig. 5. Temporal windowing concept. It is possible to eliminate the spikes in the seed signal by using a temporal window positioned after the bandstop filter as indicated in the figure. This can be practically implemented by delaying the electron bunch at the position where the frequency spectrum of the transmitted X-ray pulse experiences a strong temporal separation.

however, requires a correction when the incident beam almost satisfies the Bragg diffraction condition and multiple scattering takes place. Usually, X-ray multiple scattering in a perfect crystal is described by the dynamical theory of X-ray diffraction [21]. According to this theory, when the incident angle is near the diffraction condition, the transmittance spectrum of a thick crystal shows an absorption line with a narrow width, which is close to the line width in the reflectance spectrum for the case of small absorption influence. In this paper we will discuss only the case for small absorption: in particular, we will consider the C(400) reflection of 0.15 nm X-ray from a 0.1 mm-thick diamond plate, see Fig. 2. When the incident angle and the spectral contents of the incoming beam satisfies the Bragg diffraction condition, the temporal waveform of the transmitted radiation pulse shows a long monochromatic wake. The duration of this wake is inversely proportional to the bandwidth of the absorption line in the transmittance spectrum. Then, the single crystal in Bragg geometry actually operates as a bandstop filter for the transmitted X-ray SASE radiation pulse, see Fig. 4. Obviously, if we use a bandstop filter there is no monochromatization in the frequency domain. However, it is possible to reach a bandwidth limited seed signal by using a temporal window positioned after the bandstop filter as indicated in Fig. 5. In the XFEL case we deal with a parametric amplifier where the properties of the active medium, i.e. electron beam, depend on time. As a result, the temporal windowing concept can be practically implemented in a simple way by delaying the electron bunch at the position where the

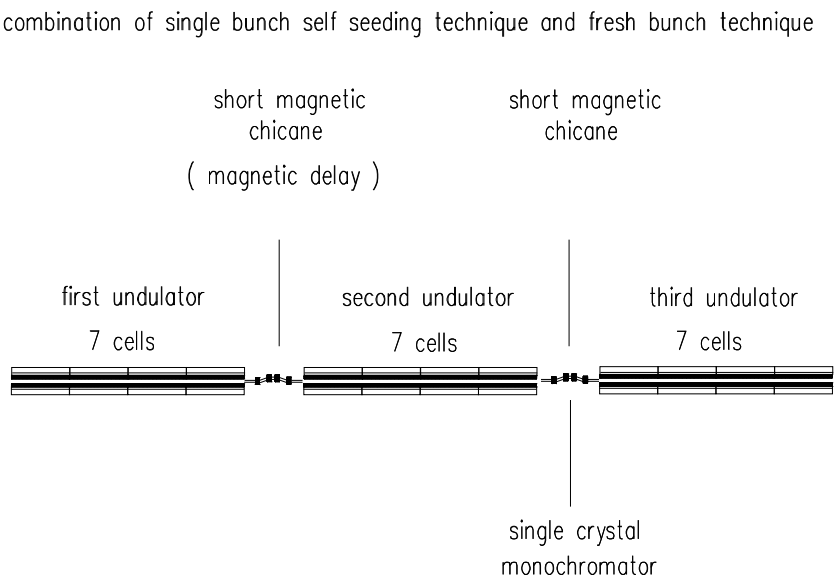

Fig. 6. Design of an undulator system for the narrow bandwidth mode of operation. The method exploits a combination of a single bunch self-seeding scheme, based on the use of a single crystal monochromator and of a temporal windowing technique, and of a fresh bunch scheme.

frequency spectrum of the transmitted X-ray pulse experiences a strong temporal separation. In other words, the magnetic chicane in Fig. 3 shifts the electron bunch on top of the monochromatic wake created by the bandstop filter. By this, it is possible to seed the electron bunch with a radiation pulse characterized by a bandwidth much narrower than the natural FEL bandwidth. In the proposed scheme, no time dependent elements are used and problems with synchronization and time jitter do not exist at all.

3 Combination of self-seeding and fresh bunch techniques

In this section we will discuss how the above-described method may be combined with a fresh bunch technique [16]-[20]. The idea is sketched in Fig. 6, Fig. 7, and Fig. 8. The scheme can be practically realized by using three undulator parts, Fig. 6. The first undulator operates in the linear high-gain regime starting from the shot noise in the electron beam. After the first undulator, the electron bunch is sent to a short magnetic chicane, which removes the microbunching and introduces a delay of the electron bunch with respect to the radiation pulse, Fig. 7. In this way, half of the electron bunch is seeded, and saturates in the second part of the undulator. Note that for European XFEL or LCLS parameters, microbunching is washed out already with a small dispersive strength R_{56} in the order of ten microns, allowing for a short 5 m-long chicane to be installed in place of a single

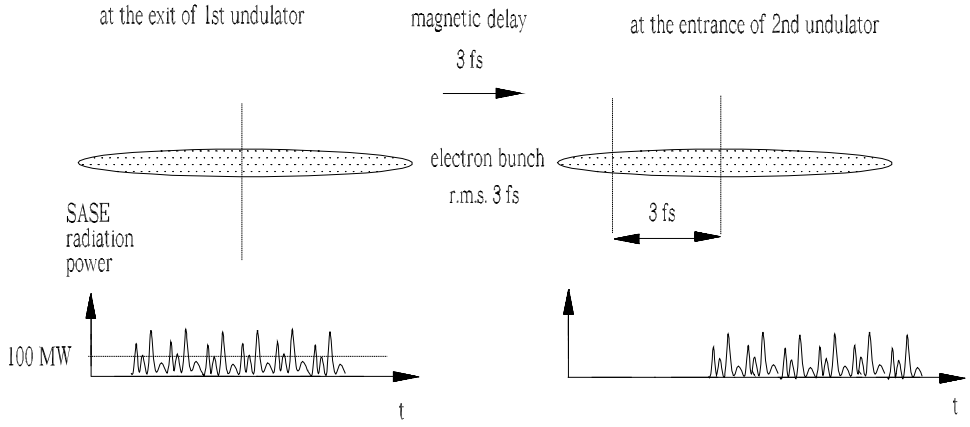

Fig. 7. Sketch of principle of the fresh bunch technique for the short (6 fs) pulse mode of operation.

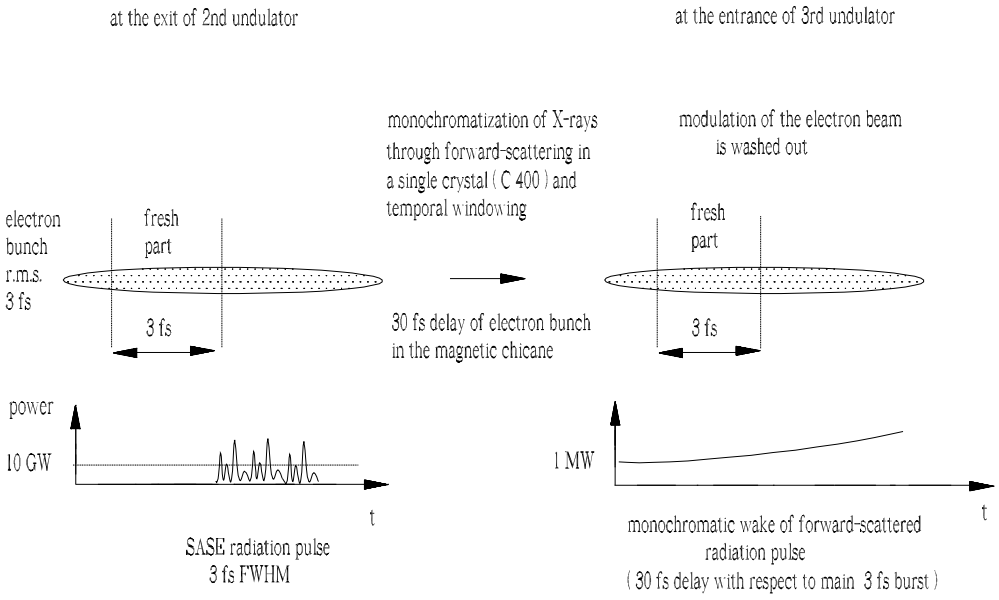

Fig. 8. Sketch of the X-ray monochromatization principle from the second to the third undulator. By using a combination of a fresh bunch technique and a single-bunch self-seeding technique, based on the use of a single crystal monochromator and of the temporal windowing operation, a MW-level monochromatic wake of radiation can be produced behind the monochromator.

undulator module. After the second undulator the electron bunch is sent to a second magnetic chicane, Fig. 8, and the strong radiation pulse impinges on a crystal set for Bragg diffraction. The refracted radiation pulse seeds the remaining fresh part of the delayed electron bunch, thus implementing

the temporal windowing technique, and is amplified up to saturation in the third part of the undulator. In this scheme, the mean value of the radiation power after the crystal within the temporal window will be in the few MW level. This is the input radiation power at the entrance of the third undulator, and is much larger than the shot noise power (3 kW).

The combination of self-seeding and fresh bunch techniques is extremely insensitive to noise and non-ideal effects. In fact, the radiation pulse used to produce the monochromatic wake is in the GW level power. This large power can tremendously improve the signal to noise ratio of the self-seeding scheme. It should be remarked that the possibility of combining self-seeding scheme and fresh bunch technique would be especially of great importance during the early experimental stage, when a proof of principle is built. During this stage all non ideal effects can be reduced to a minimum. After this stage, one may implement other self-seeding schemes based on the wake monochromator.

The advantage of our novel self-seeding method is a minimal hardware requirement, consisting in the installation of two short magnetic chicanes as shown in Fig. 6. These chicanes do not perturb the undulator focusing system and do not interfere with the baseline mode of operation. Our three stage self-seeding scheme is therefore compatible with the baseline design of the European XFEL [1].

4 Transmissivity relevant to Bragg diffraction

Consider the forward-scattered X-rays produced in the transmission direction when an X-ray beam is directed upon a crystal. As discussed before, when the incident beam almost satisfies the Bragg reflection condition, multiple scattering takes place and the phase shift acquired by the forward-scattered X-ray pulse with respect to the incident pulse requires corrections to account for this effect. If we know the modulus of the transmittance of the crystal T we can find the minimal phase shift of the forward-scattered X-ray pulse with the help of Kramers-Kronig relations.

Usually, X-ray multiple scattering in a perfect crystal is described by the dynamical theory of X-ray diffraction (see e.g. [21] for a comprehensive treatment). Let us first illustrate and test the method of phase determination based on the Kramers-Kronig relations in the case of the reflectance for a thick crystal. In doing this we will account for the well-known result of dynamical theory that the modulus of the reflectance has no zeros in the complex plane and, thus, the minimal phase solution equals the total phase. According to the dynamical theory of diffraction, when the incident angle

is in the vicinity the diffraction condition, and one neglects absorption, the reflectance for a thick crystal is analytically given by

$$Z(\eta) = \left| \eta \pm \sqrt{\eta^2 - 1} \right| \tag{1}$$

$$\Phi(\eta) = \arg\left[-\eta + \sqrt{\eta^2 - 1} \right] . \tag{2}$$

Eq. (1) and Eq. (2) constitute an analytical expression for the crystal rocking curve. Here the positive or negative sign in Eq. (1) should be taken such that $Z < 1$. In literature η is known as the deviation parameter. When absorption is neglected, such parameter varies from -1 to $+1$ when the reflectivity is 100%. Note that in our case of interest we have an angular divergence of the incident photon beam about a microradiant, which is much smaller than the Darwin width of the rocking curve ($10 - 15\mu$rad.) Therefore, we assume that all frequencies impinge on the crystal at the same angle. When this incident angle is in the vicinity of the Bragg diffraction condition, multiple scattering takes place. However, mirror reflection takes place for all frequencies. Therefore, the reflected beam has exactly the same divergence as the incoming beam. The reflectivity coefficient is described by a reflectivity curve, which can be extracted from the rocking curve of the crystal and from the knowledge of the Bragg angle. The incident angle of the X-ray beam which is interpreted as Bragg angle determines the position of the reflectivity curve along the frequency axis. Multiplication of η by the bandwidth $\Delta\omega_{nkl}/\omega$, which depends on the reflection, yields the reflectivity curve and the phase as a function of the deviation from the center of reflectivity curve, $\Delta\omega/\omega = \eta\Delta\omega_{nkl}/\omega$. Thus, in our case we can say that η represents a reduced frequency deviation [2], and we can rewrite Z and Φ as a function of ω.

$Z(\omega)$ and $\Phi(\omega)$ may thus be regarded as modulus and phase of a linear filter in the frequency domain. Despite the numerous achievements of the dynamical theory of diffraction it has never been considered, at least to our knowledge, that the phase of this filter, $\Phi(\omega)$, can be recovered from the knowledge of the modulus $Z(\omega)$ alone just by exploiting causality and square-integrability, which are both obvious physical requisites, yielding an

[2] It may be worth to note here that usually one is interested in the reflectivity curve, at a fixed frequency of incident radiation, as a function of the deviation from the Bragg's angle. Here, instead, we consider the reflectivity at the Bragg's angle corresponding to a given frequency ω and we scan the frequency $\Delta\omega$ at a fixed angle.

interesting relation between dynamical theory of diffraction and Kramers-Kronig relations.

In fact, according to Titchmarsch theorem (see [22] for a review on the subject) causality [3] and square-integrability of the inverse Fourier transform of $\bar{F}(\omega) = Z\exp(i\Phi)$, which will be indicated with $F(t)$, is equivalent to the existence of an analytic continuation of $Z\exp(i\Phi)$ to $\Omega = \omega + i\omega'$ on the upper complex Ω-plane (i.e. for $\omega' > 0$). The same theorem, also shows that the two previous statements are equivalent to the fact that real and imaginary part of $\bar{F}(\omega)$ are connected by Hilbert transformation. Since $F(t)$ must be real (thus implying that $\bar{F}^*(\omega) = \bar{F}(-\omega)$), from the Hilbert transformation follow the well-known Kramers-Kroninig relations [23, 24]:

$$\begin{aligned} \mathrm{Re}[\bar{F}(\omega)] &= \frac{2}{\pi}\mathcal{P}\int_0^\infty \frac{\omega'\mathrm{Im}[\bar{F}(\omega')]}{\omega'^2-\omega^2}d\omega' \\ \mathrm{Im}[\bar{F}(\omega)] &= -\frac{2}{\pi}\mathcal{P}\int_0^\infty \frac{\mathrm{Re}[\bar{F}(\omega')]}{\omega'^2-\omega^2}d\omega' \ , \end{aligned} \tag{3}$$

linking real and imaginary part of $\bar{F}(\omega)$. A similar reasoning can be done for the modulus $Z(\omega)$ and the phase $\Phi(\omega)$, see [25]. In fact, one can write

$$\ln[\bar{F}(\omega)] = \ln[Z(\omega)] + i\Phi(\omega) \ . \tag{4}$$

Note that $\bar{F}^*(\omega) = \bar{F}(-\omega)$ implies that $|\bar{F}(\omega)| = |\bar{F}(-\omega)|$ and that $\Phi(\omega) = -\Phi(-\omega)$. Therefore, using Eq. (4) one also has that $\ln[\bar{F}(\omega)]^* = \ln[\bar{F}(-\omega)]$. Then, similarly as before, application of Titchmarsh theorem shows that the analyticity of $\ln[Z(\Omega)]$ on the upper complex Ω-plane implies that

$$\Phi(\omega) = -\frac{2}{\pi}\mathcal{P}\int_0^\infty \frac{\ln[Z(\omega')]}{\omega'^2-\omega^2}d\omega' \ , \tag{5}$$

One may verify that a direct use of Eq. (5), with Z given as in Eq. (1), yields back the phase $\Phi(\omega)$. It is important to note, however, that in applying such procedure we tacitly assumed that $\ln[Z(\Omega)]$ is analytical on the upper complex Ω-plane. While causality implies this fact for $\bar{F}(\Omega)$, this is not the case,in general, for $\ln[Z(\Omega)]$. In fact, such function is singular where $\bar{F}(\Omega) = 0$. In the case under discussion, one can retrieve $\Phi(\omega)$ only because $\bar{F}(\Omega) > 0$

[3] Causality simply requires that the filter can respond to a physical input after the time of that input and never before.

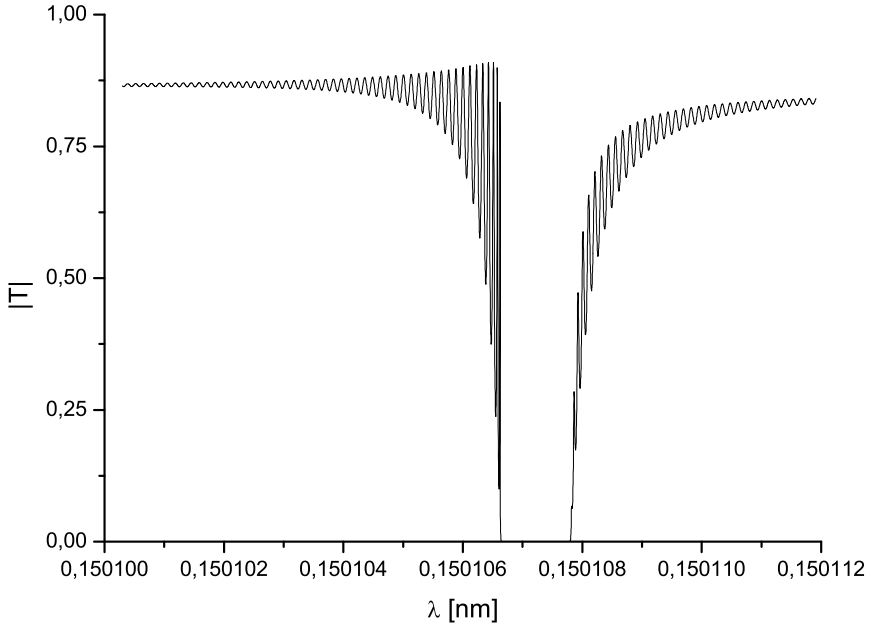

Fig. 9. Transmissivity (sigma polarization) relevant to the Bragg 400 diffraction of X-rays at 0.15 nm from a Diamond crystal with a thickness of 0.1 mm.

everywhere on the complex plane, as it can be seen taking the analytic continuation of $\bar{F}(\omega)$ defined by Eq. (1) and Eq. (2). Note, however, that the knowledge of this fact comes as a consequence of diffraction theory. Without such information we would be able to go through the same algorithm, but we would not be certain that Eq. (5) really yields back $\Phi(\omega)$. If $\bar{F}(\omega)$ had zeros on the upper complex plane, these zeros would have contributed adding extra terms to the total phase. For this reason, Eq. (5) is known as minimal phase solution.

Let us now consider the phase shift of the forward-diffracted X-rays by a crystal with absorption. We first used the dynamical theory of diffraction to evaluate the transmittance in Bragg geometry. Fig. 9 gives the transmissivity curve for a thick (0.1 mm) absorbing crystal in Bragg geometry for the Diamond 400 reflection [26]. We subsequently used the modulus of the transmittance in Fig. 9, and we used the software in [27], accompanying reference [22], to retrieve the minimal phase solution according to Eq. (5). The result, which will be used in the following sections, is shown in Fig. 10.

Finally, it is important to remark that the reconstructed phase shift satisfies causality, meaning that we found a causal solution for the transmitted X-rays. Without taking into account the phase shift of our transmitted pulse, causality would be obviously violated. We combined dynamical theory and Kramers-Kronig relations for the first time to our knowledge. This

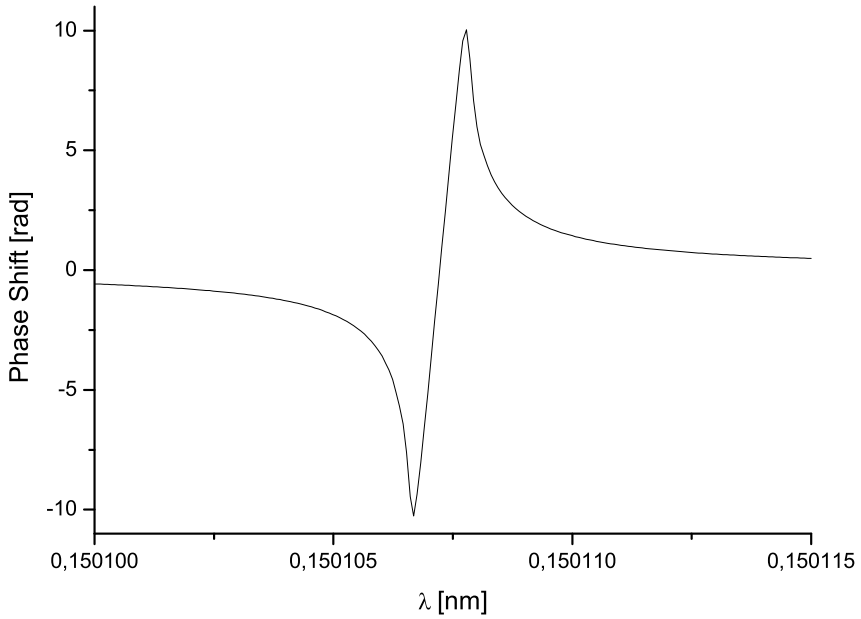

Fig. 10. Minimal phase shift of the forward-diffracted X-rays at 0.15 nm (sigma polarization) relevant to the Bragg 400 diffraction from a Diamond crystal with a thickness of 0.1 mm. The phase shift is reconstructed by Kramers-Kronig transformation Eq (5).

combination may also be used for other purposes, for example to check numerical calculations based on the dynamical theory of X-ray diffraction. One may now check the shape of real and imaginary parts of reflectance and transmittance in relation with causality.

5 Feasibility study

Following the introduction of the proposed methods we report on a feasibility study of the single-bunch self-seeding scheme with a wake monochromator. This feasibility study is performed with the help of the FEL code GENESIS 1.3 [28] running on a parallel machine. In the next subsection we will present the feasibility study for the short-pulse mode of operation (6 fs), while, later on, we will cover the long-pulse mode of operation (60 fs). Parameters used in simulations for the short pulse mode of operations are presented in Table 1. For the long pulse mode of operations Table 1 is still valid, except for a ten times larger charge (0.25 nC) and a ten times longer rms bunch length (10μm, corresponding to 60 fs). In both cases we use a combination of the fresh bunch technique and the wake monochromator

Table 1
Parameters for the short pulse mode of operation used in this paper.

	Units	
Undulator period	mm	48
K parameter (rms)	-	2.516
Wavelength	nm	0.15
Energy	GeV	17.5
Charge	nC	0.025
Bunch length (rms)	μm	1.0
Normalized emittance	mm mrad	0.4
Energy spread	MeV	1.5

method, shown in Fig. 6. Details on the operation of the fresh-bunch technique and its combination with the self-seeding technique are discussed in [11], and the first two undulator parts considered in that reference are exactly the same used here.

5.1 Feasibility study for the short pulse mode of operation

We begin with Fig. 11, where we present the output at the end of the second stage, i.e. after the application of the fresh-bunch technique. We take this result as our starting point without further comments, since Fig. 11 has already been introduced and thoroughly discussed in [11].

As explained before, the crystal acts as a bandstop filter. Such effect is best shown in terms of the spectrum in Fig. 12, where we show a comparison between spectra before and after the filter. The effect is highlighted in the inset. The corresponding power is shown in Fig. 13. As discussed before, monochromatization does not take place in the frequency domain. At first glance, the passage through the bandstop filter is only responsible for slight changes in the power distribution along the pulse. However, a zoom of the vertical axis shows what we are interested in: a long, monochromatic tail in the power distribution on the left side of the picture, Fig. 14. Note that there is no corresponding tail on the right side of Fig. 14. This fact is consistent with causality. This fact is evident from the analysis of Fig. 15, which illustrates the power distribution before and after the filter in logarithmic scale. It is interesting to compare Fig. 15 with what would have been obtained in the case we completely neglected the phase in the transmittance T. In this case, instead of Fig. 15 we would have obtained Fig. 16. It is interesting to see that even without phase we can rely on sufficient

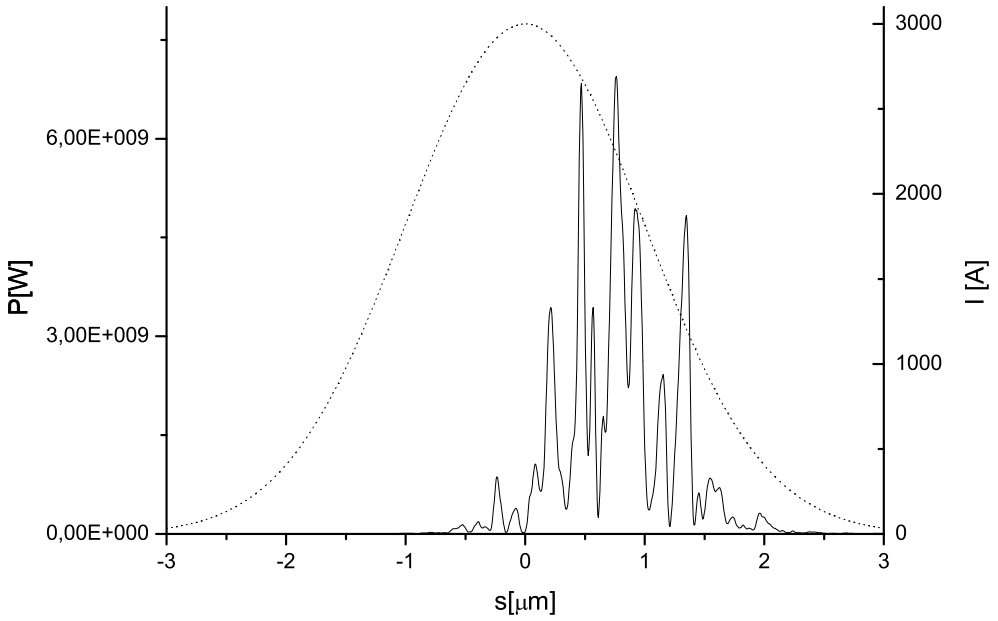

Fig. 11. Short pulse mode of operation, combination of self-seeding and fresh bunch techniques. Output power at the end of the second stage, 7 cells long (42 m). The dashed line illustrates the corresponding distribution of the electron beam current.

power for seeding. However, we would have strongly underestimated it of about a factor 10. Moreover, as expected, Fig. 16 shows a non-causal behavior of the signal. This is evident from the analysis of Fig. 15, where we compare the power after transmission with and without phase, and the power before transmission in logarithmic scale. The large jump between the power after transmission accounting for the phase is due to causality. Data without phase show, instead, a symmetric behavior, which is not causal at all. The very small ($\sim 10^{-4}$) but visible departures from the exact zero result appear in the right-hand side of the picture in logarithmic scale, Fig. 15. This accuracy is acceptable for most purposes.

Inspection of Fig. 14 shows that the seeding power in the monochromatic tail is about 10 MW. It should be noted that this power is about three orders of magnitude larger than the shot noise power. Moreover, within the temporal window that used (3 fs, corresponding to about 1μm in the plot), the seed power is practically constant along the bunch and fluctuates according to a negative exponential function i.e. as the instantaneous power (note that even for 100% fluctuations we always have the seed power much larger than the shot noise power). As a result, we do not need to average over many shots, when considering our feasibility study. It follows that the combination of our new self-seeding technique with the fresh bunch technique is particularly

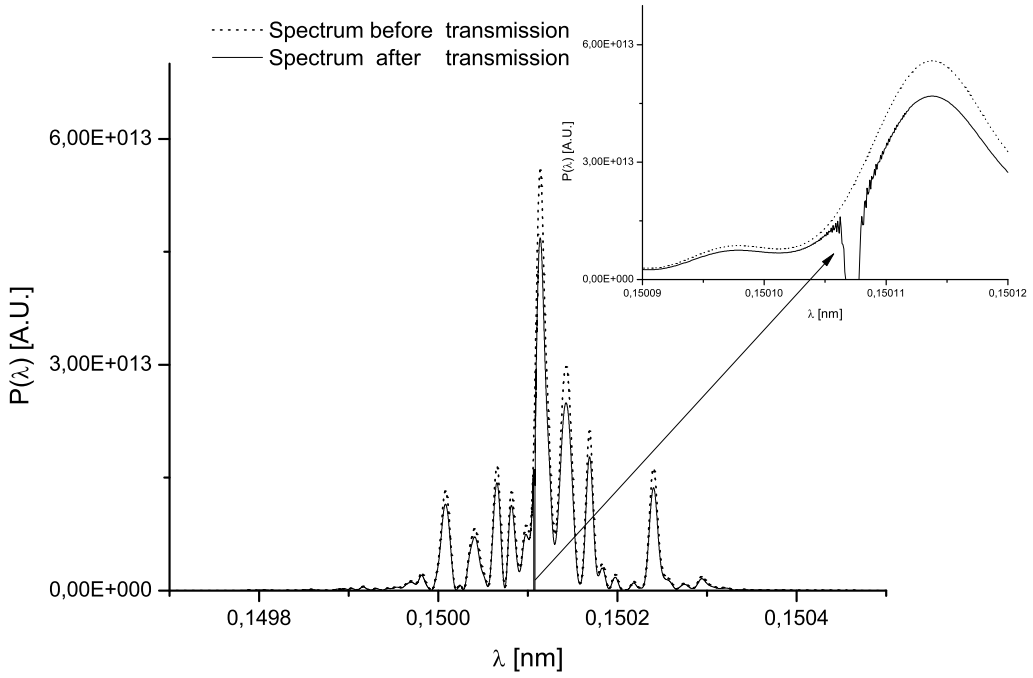

Fig. 12. Short pulse mode of operation, combination of self-seeding and fresh bunch techniques. Output spectrum after the diamond crystal. The bandstop effect is clearly visible, and highlighted in the inset. For comparison, the spectrum before transmission (dotted line) is superimposed to the spectrum after transmission (solid line).

well-suited for demonstrating the feasibility of our technique in a simple but sure way. The fresh part of the bunch is seeded by such monochromatic tail, and the monochromatic signal is amplified up to saturation in the last undulator part, which is 7 cells long. The final output is shown in Fig. 17 and Fig. 18, which show both spectrum and power distribution after the third undulator stage. The relative spectral width is $8 \cdot 10^{-5}$ and is near to the transform-limited bandwidth of a Gaussian pulse with the same FWHM.

In closing, it should be noted that the feasibility of the method is not really sensitive on the phase of the transmittance. In other words, even for the (non-physical) choice of zero phase, one would obtain a sufficient seed power to demonstrate the feasibility of the method.

5.2 Feasibility study for the long pulse mode of operation

Let us now consider the case of long pulse mode of operation. Similarly as before, in Fig. 19 we present the input power. Subsequently, a comparison between the spectrum before and after transmission is shown in Fig. 20.

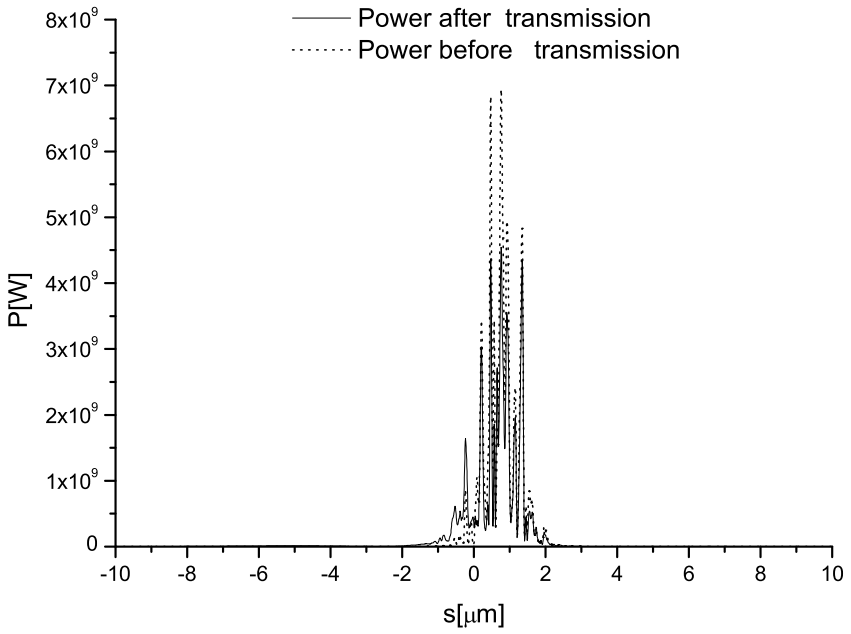

Fig. 13. Short pulse mode of operation, combination of self-seeding and fresh bunch techniques. Power distribution before (dotted line) and after (solid line) transmission through the crystal.

The bandstop effect is clearly visible in the inset. In this case we still used the C(400) reflection. Note that the width of the reflectivity curve is now comparable with the spike width in the frequency domain. Thus, in contrast to the short-pulse case, the characteristic scale of the tail length, which is the inverse line width of the filter, is comparable with the radiation pulse duration and with the electron bunch duration, which is even two times longer. Therefore, it is not trivial to understand how the self-seeding process takes place. The answer is found by inspection of Fig. 20. The reflectivity curve is, in fact, very sharp, compared with the spectrum distribution shape. As a result the monochromatic tail is much longer than the inverse width of the reflectivity curve. The power distribution is shown in Fig. 21, and the monochromatic tail is well-visible in the zoom of that plot, Fig. 22.

The final output is shown in Fig. 23 and Fig. 24, which illustrate both spectrum and power distribution after the third undulator stage. The relative spectral width is about 10^{-5}.

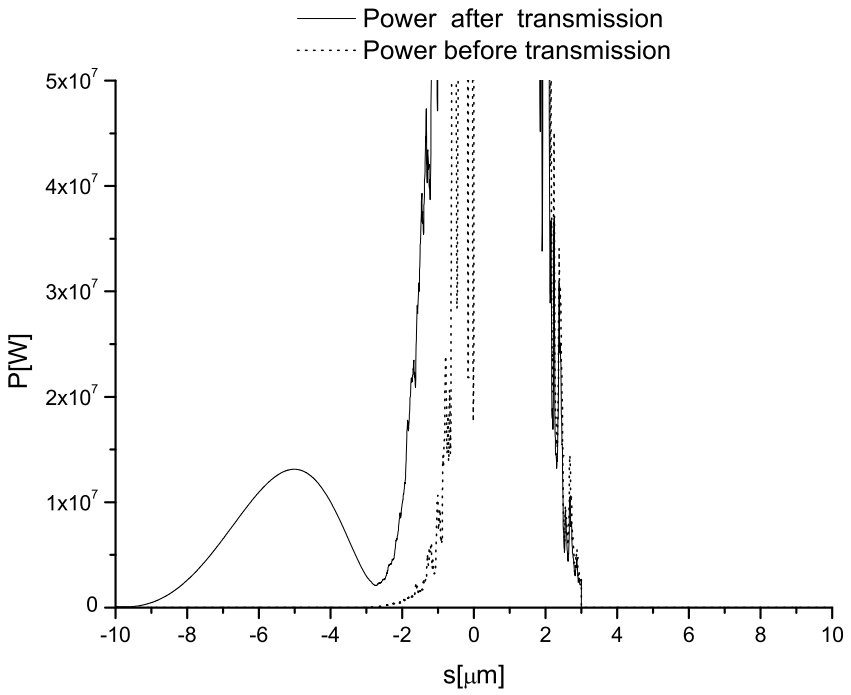

Fig. 14. Enlargement of Fig. 13. The horizontal axis is left unchanged, while the vertical axis is zoomed. The monochromatic tail due to the transmission through the bandstop filter is now evident on the left of the figure.

6 Conclusions

In this paper we propose a novel scheme to produce highly monochromatic X-rays from a baseline SASE XFEL, down to a relative bandwidth of 10^{-5}. The key components of such scheme include only a single crystal and a short magnetic chicane with very small offset. A distinguishing feature of our method is that it uses a single crystal in the transmission direction, instead of a fixed-exit four-crystal monochromator. As a result, the X-ray optics is extremely simple to align: it involves no beam-recombining and no scanning of the delay. The alignment tolerance of the crystal angle is expected to be in the range of a fraction of mrad for fitting the Bragg reflectivity line to the SASE XFEL radiation bandwidth.

We first illustrated the method, stressing for the first time to our knowledge the link between the dynamical theory of diffraction and Kramers-Kronig relations when dealing with the calculation of the phase shift for the forward-diffracted beam in Bragg geometry. Subsequently, we presented a feasibility study of the proposed technique for both short and long pulse mode of operation.

A great advantage of our method is that it includes no path delay of X-

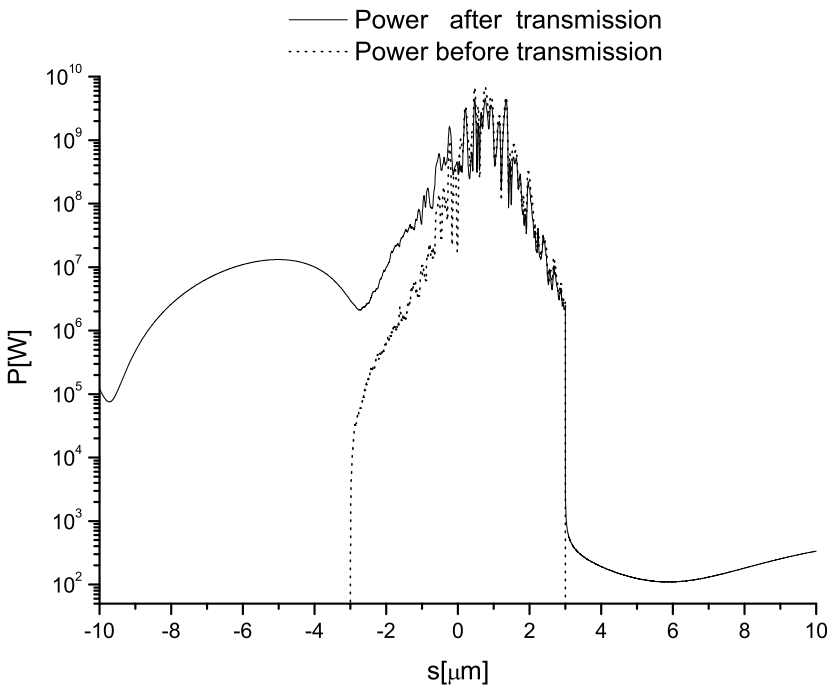

Fig. 15. Short pulse mode of operation, combination of self-seeding and fresh bunch techniques. Output power after the diamond crystal in logarithmic scale. Power distribution after transmission through the crystal, accounting for the transmission phase.

rays in the monochromator. This fact eliminates the need for a long electron beam bypass, or for the creation of two precisely separated, identical electron bunches, as required in previously proposed self-seeding schemes. The present scheme is therefore inexpensive and compact. Moreover, the proposed combination of single crystal and weak chicane allows for a straightforward installation of the self-seeding setup in the baseline undulator system, already during the commissioning phase of SASE2 at the European XFEL, and can become operational by the end of 2014.

7 Acknowledgements

We are grateful to Massimo Altarelli, Reinhard Brinkmann and Serguei Molodtsov for their support and their interest during the compilation of this work, to Martin Tolkiehn and Edgar Weckert for useful discussions.

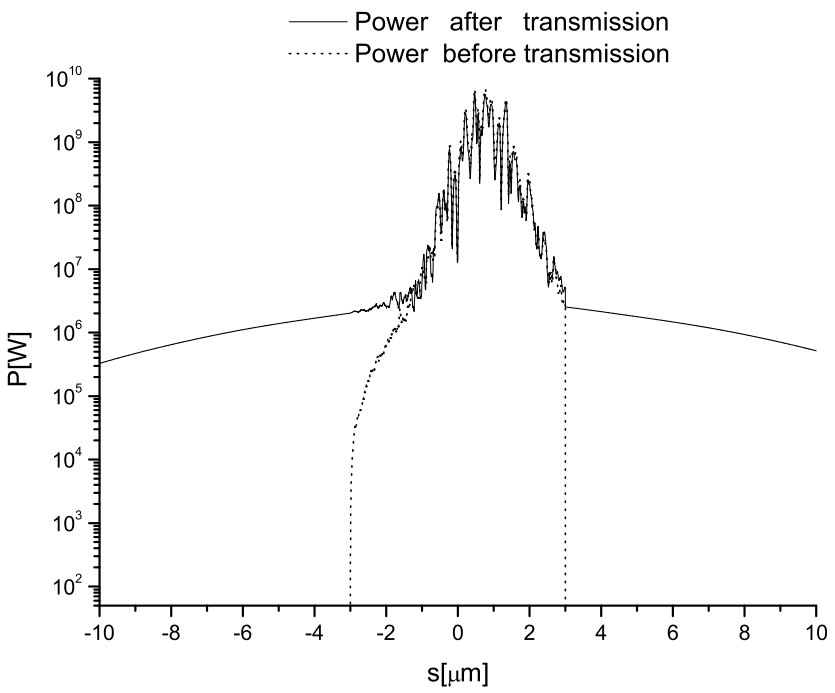

Fig. 16. Short pulse mode of operation, combination of self-seeding and fresh bunch techniques. Output power after the diamond crystal in logarithmic scale. Power distribution after transmission through the crystal, not accounting for the transmission phase.

References

[1] M. Altarelli, et al. (Eds.) XFEL, The European X-ray Free-Electron Laser, Technical Design Report, DESY 2006-097, Hamburg (2006).

[2] J. Arthur et al. (Eds.) Linac Coherent Light Source (LCLS). Conceptual Design Report, SLAC-R593, Stanford (2002) (See also http://www-ssrl.slac.stanford.edu/lcls/cdr).

[3] P. Emma, First lasing of the LCLS X-ray FEL at 1.5 Å, in Proceedings of PAC09, Vancouver, to be published in http://accelconf.web.cern.ch/AccelConf/ (2009).

[4] Y. Ding et al., Phys. Rev. Lett. 102, 254801 (2009).

[5] T. Tanaka et al. (Eds.) Spring-8 Compact SASE Source Conceptual Design report, Kouto (2005) (See also http://www-xfel.spring8.or.jp/SCSSCDR.pdf)

[6] J. Feldhaus et al., Optics. Comm. 140, 341 (1997).

[7] E. Saldin, E. Schneidmiller, Yu. Shvyd'ko and M. Yurkov, NIM A 475 357 (2001).

[8] E. Saldin, E. Schneidmiller and M. Yurkov, NIM A 445 178 (2000).

[9] R. Treusch, W. Brefeld, J. Feldhaus and U Hahn, Ann. report 2001 "The seeding project for the FEL in TTF phase II" (2001).

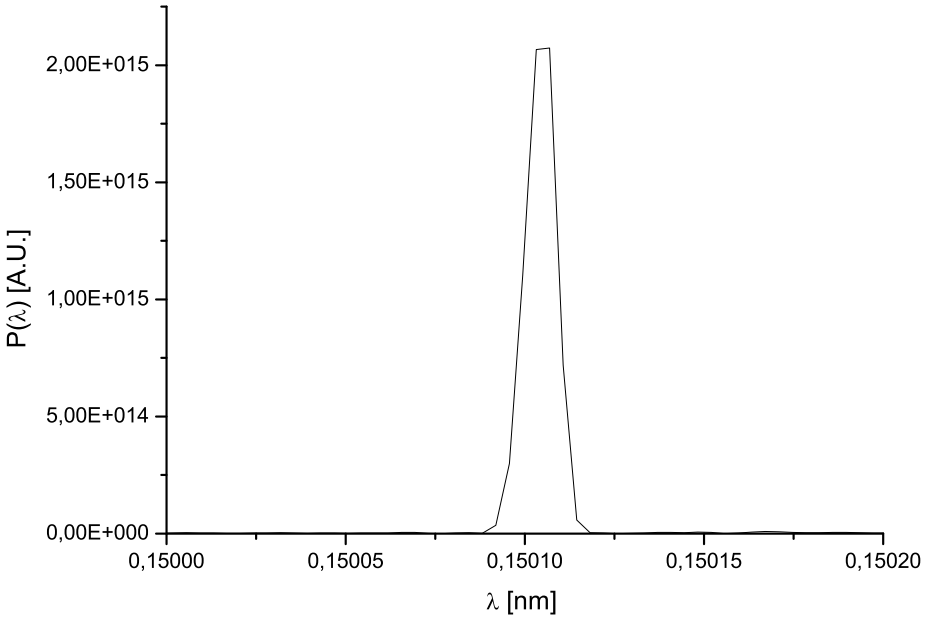

Fig. 17. Short pulse mode of operation, combination of self-seeding and fresh bunch techniques. Output spectrum of the device. The relative spectral width is $5 \cdot 10^{-5}$ and is close to the transform limit.

[10] A. Marinelli et al., Comparison of HGHG and Self Seeded Scheme for the Production of Narrow Bandwidth FEL Radiation, Proceedings of FEL 2008, MOPPH009, Gyeongju (2008).
[11] G. Geloni, V. Kocharyan and E. Saldin, "Scheme for generation of highly monochromatic X-rays from a baseline XFEL undulator", DESY 10-033 (2010).
[12] O. Grimm, K. Klose and S. Schreiber, Double-pulse Generation with the FLASH Injector Laser for Pump-Probe Experiments, Proceedings of EPAC 2006, THPCH150, Edimburgh (2006).
[13] I. Ben-Zvi and L.H. Yu, Nucl. Instr. and Meth. A 393, 96 (1997).
[14] E. Saldin, E. Schneidmiller and M. Yurkov, Opt. Commun. 212, 377 (2002).
[15] E. Saldin, E. Schneidmiller and M. Yurkov, Opt. Commun., 239, 161 (2004).
[16] G. Geloni, V. Kocharyan and E. Saldin, "Scheme for femtosecond-resolution pump-probe experiments at XFELs with two-color ten GW-level X-ray pulses", DESY 10-004 (2010).
[17] G. Geloni, V. Kocharyan and E. Saldin, "The potential for extending the spectral range accessible to the European XFEL down to 0.05 nm", DESY 10-005 (2010).
[18] G. Geloni, V. Kocharyan and E. Saldin, "Scheme for simultaneous gen-

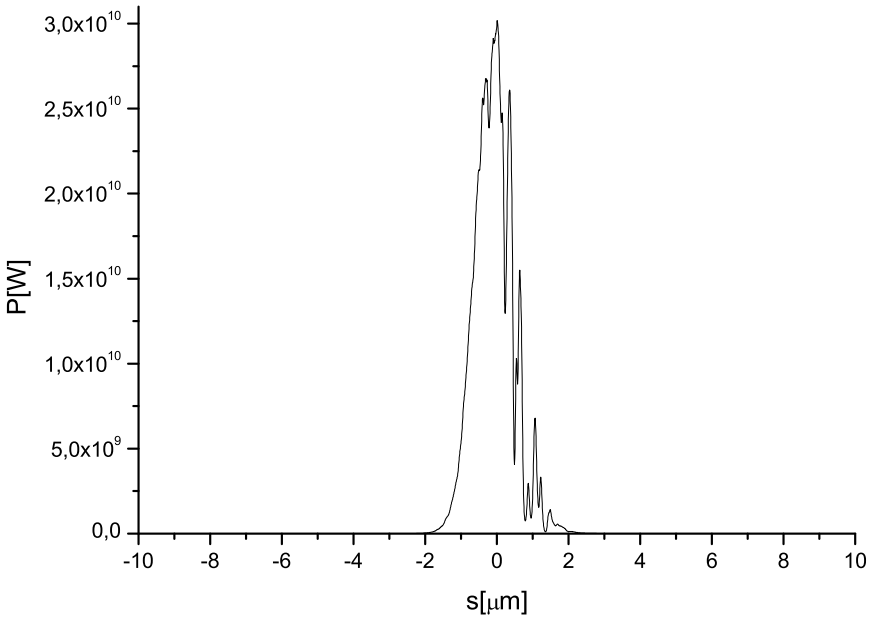

Fig. 18. Short pulse mode of operation, combination of self-seeding and fresh bunch techniques. Output power of the device.

eration of three-color ten GW-level X-ray pulses from baseline XFEL undulator and multi-user distribution system for XFEL laboratory", DESY 10-006 (2010).

[19] G. Geloni, V. Kocharyan and E. Saldin, "Control of the amplification process in baseline XFEL undulator with mechanical SASE switchers", DESY 10-010 (2010).

[20] G. Geloni, V. Kocharyan and E. Saldin, "Ultrafast X-ray pulse measurement method", DESY 10-008 (2010).

[21] A. Authier, Dynamical Theory of X-ray diffraction, Oxford University press (2001).

[22] V. Lucarini et al., Kramers-Kronig relations in optical materials research, Springer, (2004).

[23] H. A. Kramers, La diffusion de la lumiere par les atomes, in Atti del Congresso Internazionale dei Fisici, Vol. 2 (Zanichelli, Bologna, 1927), pp. 545 557.

[24] R. de L. Kronig, On the theory of dispersion of x-rays, J. Opt. Soc. Am. 12, 547557 (1926).

[25] J. Toll, Phys. Rev. 104, 6 (1956).

[26] E. Weckert, Private communication.

[27] V. Lucarini, http://www.met.reading.ac.uk/~sv901069/software.html

[28] S Reiche et al., Nucl. Instr. and Meth. A 429, 243 (1999).

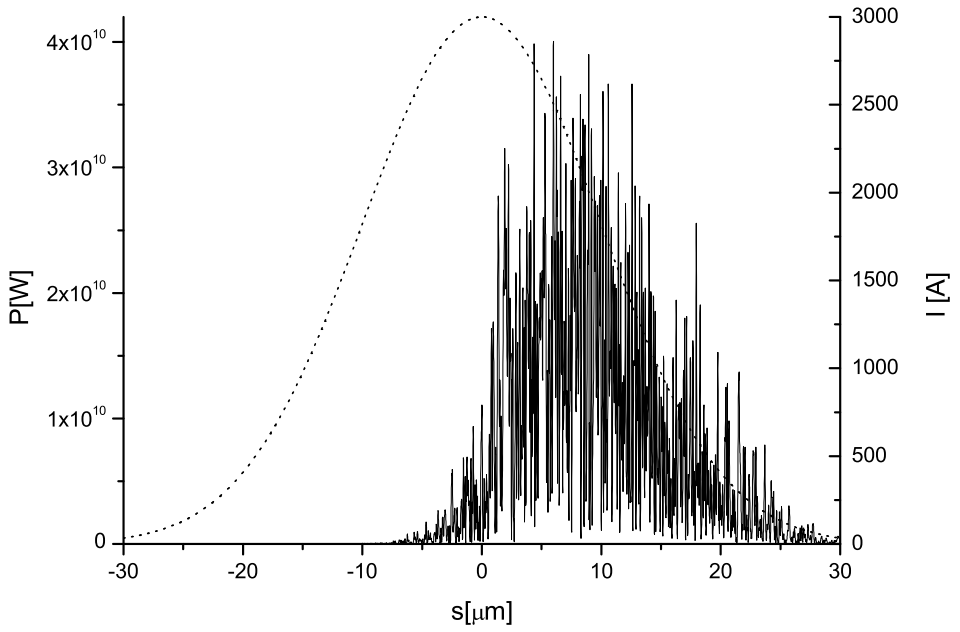

Fig. 19. Long pulse mode of operation, combination of self-seeding and fresh bunch techniques. Output power at the end of the second stage, 7 cells long (42 m). The dashed line illustrates the corresponding distribution of the electron beam current.

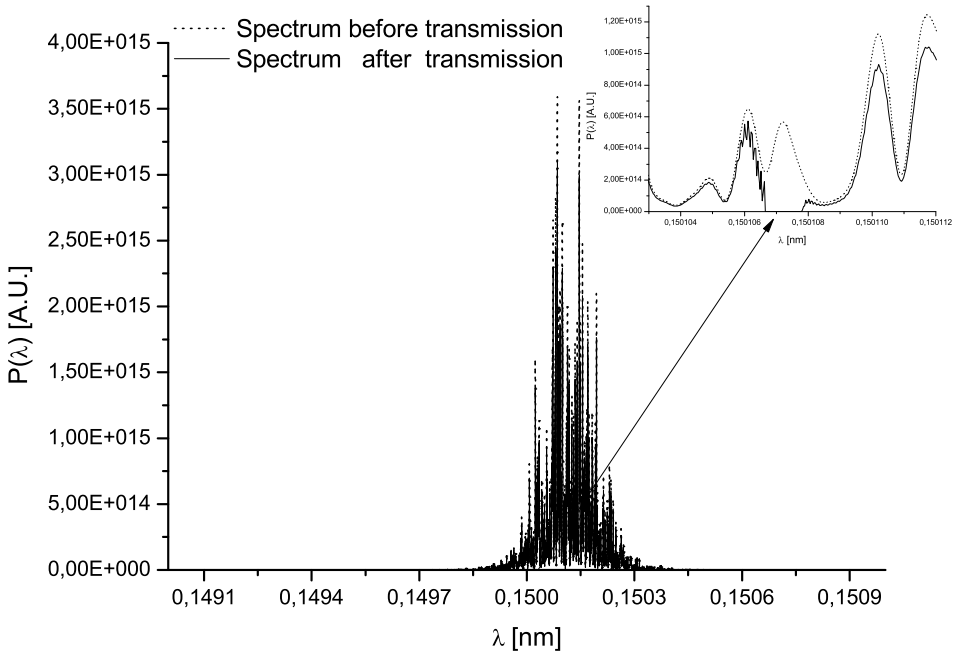

Fig. 20. Long pulse mode of operation, combination of self-seeding and fresh bunch techniques. Output spectrum after the diamond crystal. The bandstop effect is clearly visible, and highlighted in the inset. For comparison, the spectrum before transmission (dotted line) is superimposed to the spectrum after transmission (solid line).

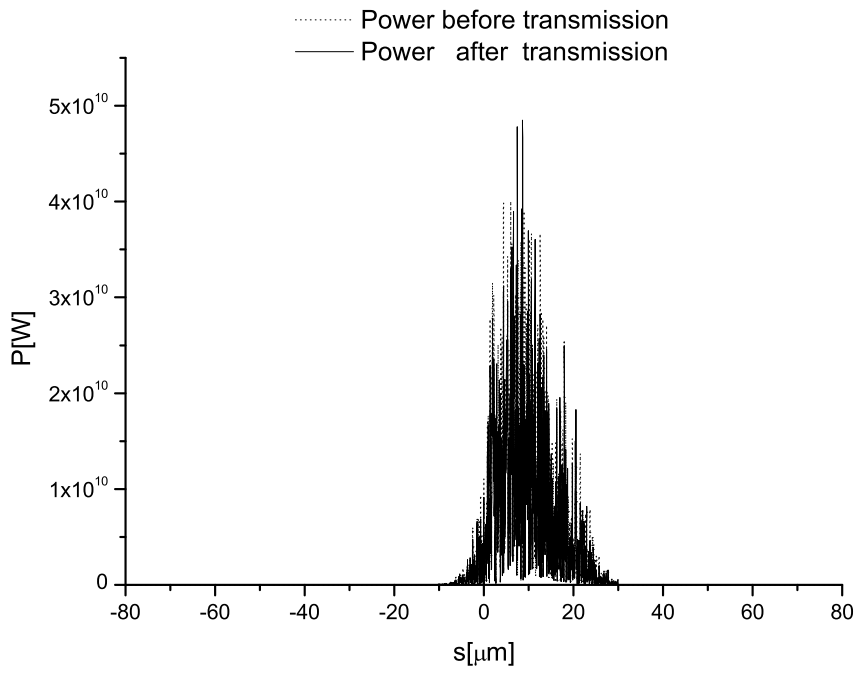

Fig. 21. Long pulse mode of operation, combination of self-seeding and fresh bunch techniques. Power distribution after transmission through the crystal.

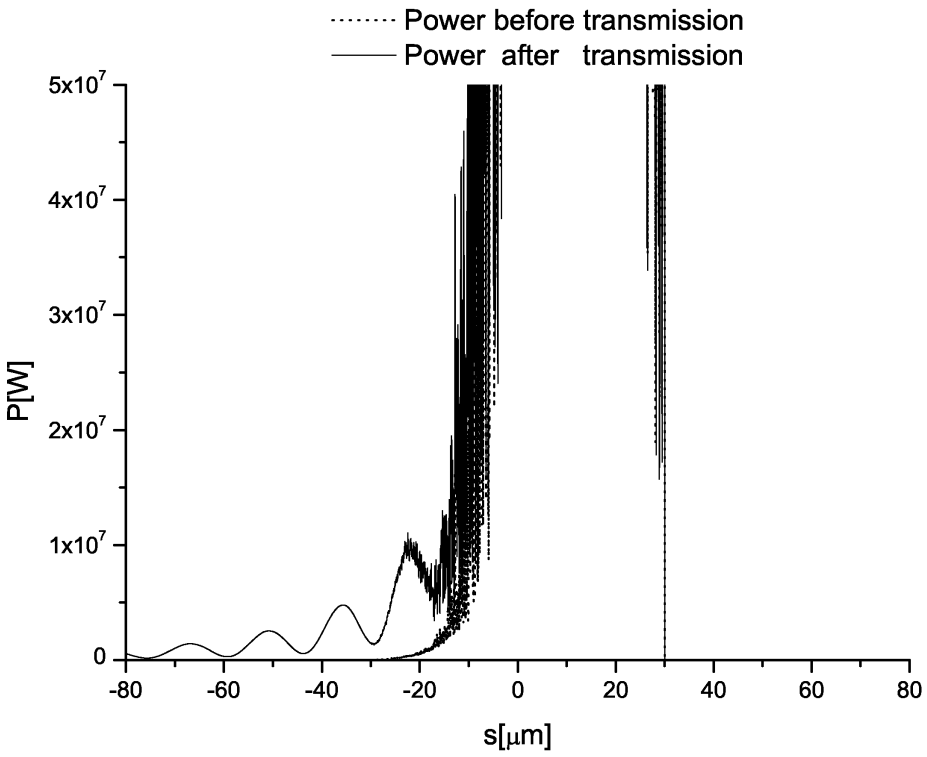

Fig. 22. Enlargement of Fig. 21. The horizontal axis is left unchanged, while the vertical axis is zoomed. The monochromatic tail due to the transmission through the bandstop filter is now evident on the left of the figure.

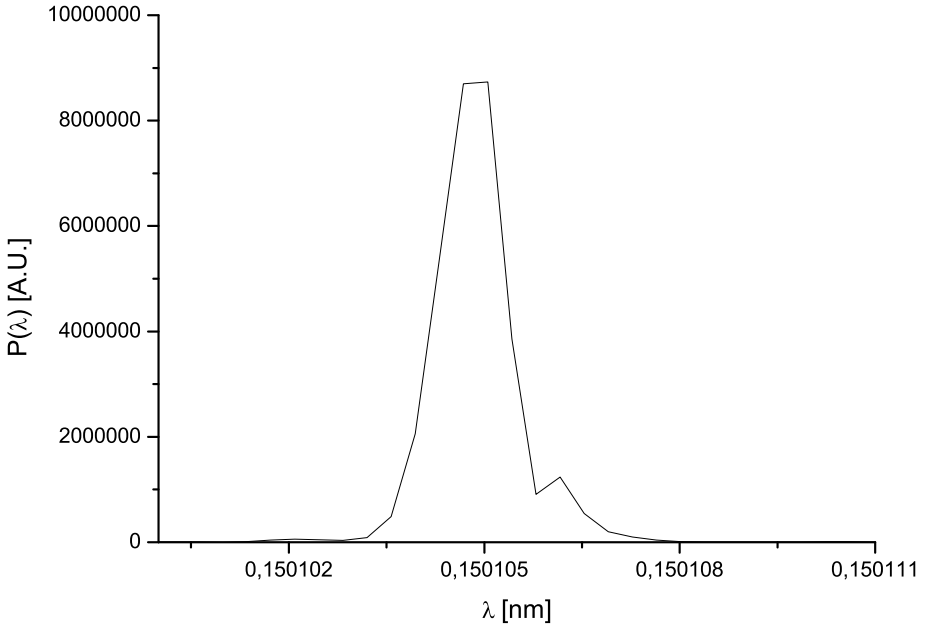

Fig. 23. Long pulse mode of operation, combination of self-seeding and fresh bunch techniques. Output spectrum of the device.

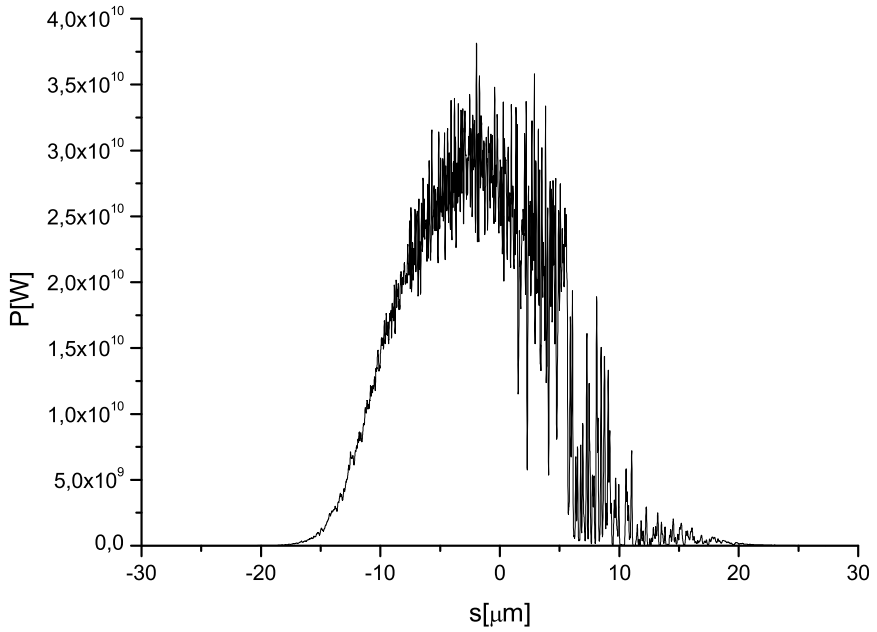

Fig. 24. Long pulse mode of operation, combination of self-seeding and fresh bunch techniques. Output power of the device.